Applied Catalysis B: Environmental 138–139 (2013) 51–61

Contents lists available at SciVerse ScienceDirect

Applied Catalysis B: Environmental

journal homepage: www.elsevier.com/locate/apcatb

Synthesis of nanosized $Ce_{0.85}M_{0.1}Ru_{0.05}O_{2-\delta}$ (M = Si, Fe) solid solution exhibiting high CO oxidation and water gas shift activity

Vijay M. Shinde, Giridhar Madras*

Department of Chemical Engineering, Indian Institute of Science, Bangalore-560 012, India

ARTICLE INFO

Article history:
Received 7 December 2012
Received in revised form 12 February 2013
Accepted 15 February 2013
Available online 21 February 2013

Keywords:
Solid solution
Ceria supported catalyst
Oxygen storage capacity
CO oxidation
Redox mechanism
Water gas shift

ABSTRACT

Nanosized $Ce_{0.85}M_{0.1}Ru_{0.05}O_{2-\delta}$ (M = Si, Fe) has been synthesized using a low temperature sonication method and characterized using XRD, TEM, XPS and H_2-TPR. The potential application of both the solid solutions has been explored as exhaust catalysts by performing CO oxidation. The addition of Si- and Fe- in $Ce_{0.95}Ru_{0.05}O_{2-\delta}$ greatly enhanced the reducibility of $Ce_{0.85}M_{0.1}Ru_{0.05}O_{2-\delta}$ (M = Si, Fe), as indicated by the H_2-TPR study. The oxygen storage capacity has been used to correlate surface oxygen reactivity to the CO oxidation activity. Both the compounds reversibly release lattice oxygen and exhibit excellent CO oxidation activity with 99% conversion below 200 °C. A bifunctional reaction mechanism involving CO oxidation by the extraction of lattice oxygen and rejuvenation of oxide vacancy with gas feed O_2 has been used to correlate experimental data. The performance of both the solid solutions has also been investigated for energy application by performing the water gas shift reaction. The present catalysts are highly active and selective towards the hydrogen production and a lack of methanation activity is an important finding of present study.

1. Introduction

Materials with high oxygen storage capacity (OSC) have attracted considerable attention due to their wide applications in auto exhaust catalysis, fuel cells and solar cells [1,2]. Ceria and ceria containing materials are promising candidates because of their excellent electrical, catalytic, and mechanical properties [3,4]. Ceria is also a major component of a three way catalyst in automotive exhaust emissions [5,6]. The facile $Ce^{4+} \leftrightarrow Ce^{3+}$ redox couple allows these materials to store and release oxygen under oxidizing and reducing conditions, respectively. The performance of these materials as catalyst depends on the OSC and the enhancement in the catalytic activity is directly correlated with increase in the OSC [7–9]. This phenomenon is well established for the reactions such as CO oxidation and water gas shift (WGS) [10–13]. Therefore, it is highly desirable to increase the active oxygen content of ceria based materials for the low temperature CO oxidation, hydrocarbon oxidation, and water gas shift (WGS) reaction.

The high OSC and oxygen mobility of ceria can be improved by modifying its structure through the doping of various cations such as Zr, Zn, Co, Cu, and Fe [14–17]. The substitution of Ti and Sn in CeO_2 forming solid solutions also increases the OSC [17–19]. However, the catalytic performance of these materials is poor at low temperatures [2]. In contrast, the Pt group (Pt, Pd, Ru and Rh) metal substituted ceria has showed high CO oxidation activity at low temperatures despite their low OSC [20]. The substitution of transition metal such as Cu, Mn, and Fe in CeO_2 results in materials that also exhibit high OSC and these catalysts have the potential to lower the cost [21–23]. The effects of the transition metal substitution on the catalytic performance of ceria have been extensively studied and very high CO oxidation activity was reported in case of Cu modified ceria [24,25].

Due to the stringent environmental regulations, there is an imperative need for more efficient and cost effective catalysts. Therefore, significant efforts has been made to explore materials with high OSC for exhaust gas purification [26]. The substitution of another metal in ceria has attracted considerable interest as a catalyst or as a promoter in many catalyst formulations [27]. The size of substituent is one of the key concepts to increase the reducibility and OSC of ceria. The substitution of cation with the smaller (ionic radius) than the Ce cation can create both short and long metal oxygen bonds. The oxygen atoms bonded to the metal with long bonds is weaker and this can increase the reducibility of ceria. This fact is well demonstrated for Ti and Zr-substituted CeO_2 solid solutions [19,28]. Previously, we have observed excellent activity of noble metal modified ceria as three way catalysts [20]. It is widely acknowledged that the aliovalent substitution of metal like Pt, Pd, Cu in CeO_2 lattice induce redox couples in both the substituted metal CeO_2 matrix renders strong metal support interactions [29–31]. Recently, the application of the periodic density functional theory (DFT) was used to demonstrate the effect of doping of

* Corresponding author. Tel.: +91 80 22932321; fax: +91 80 23601310.
E-mail addresses: giridhar@chemeng.iisc.ernet.in, giridharmadras@gmail.com (G. Madras).

0926-3373/$ – see front matter © 2013 Elsevier B.V. All rights reserved.
http://dx.doi.org/10.1016/j.apcatb.2013.02.021

various cations on the OSC of ceria and the origin of OSC was related to the oxygen vacancy formation energy [32]. In another DFT study, it has been shown that the origin of OSC of Pd/Pt doped CeO_2 lies in the extent of lattice distortions that the Pd/Pt experience within the CeO_2 lattice [33] and large distortion showed high OSC. Further, it has been shown that the dopant cations retain coordination of their own binary oxide even in ceria lattice, which gives more facile lattice oxygen than pure ceria [27]. Therefore, the reducibility of ceria depends on the extent of lattice distortion and coordination of the dopants in their native oxides.

Based on the above, we have synthesized new catalysts that are essentially a solid solution of $Ce_{0.85}M_{0.1}Ru_{0.05}O_{2-\delta}$ (M = Si, Fe) and explored their potential application for CO oxidation. The substitution of Fe and Si was rationalized based on their small ionic radii compared to host Ce ions which distort the ceria lattice and give high OSC. Ru substitution is justified based on the fact that the higher rates of CO oxidation cannot be obtained by the utilization of lattice oxygen alone and CO adsorption sites over the catalyst are essential. Therefore, in this study, we report the synthesis, structure and CO oxidation activity of $Ce_{0.85}M_{0.1}Ru_{0.05}O_{2-\delta}$ (M = Si, Fe) solid solution synthesized by low temperature sonication method. The reducibility of the catalyst was studied by temperature programmed reduction (H_2-TPR) method and the increase in the OSC was correlated to the enhancement in CO oxidation activity. The spectroscopic and experimental observation was used to describe bifunctional redox mechanism over these catalysts. Finally, we have extended the application of these materials toward the production of hydrogen by performing the WGS reaction. Both the solid solutions showed excellent activity for both the reactions.

2. Experimental

2.1. Synthesis and characterization

The solid solutions of $Ce_{0.85}M_{0.1}Ru_{0.05}O_{2-\delta}$ (M = Si, Fe) were synthesized using a low temperature sonication method. Chemical reagents including ammonium cerium nitrate (CAN) [$(NH_4)_2Ce(NO_3)_6$, S.D Fine Chem, India], tetraethyl orthosilicate (TEOS) [Merck, India], ruthenium chloride [$RuCl_3$, Spectrochem, India], and ferric nitrate [$Fe(NO_3)_3{\cdot}9H_2O$, S.D Fine Chem, India] were used as received without further purification. For the synthesis of $Ce_{0.85}Si_{0.1}Ru_{0.05}O_{2-\delta}$ solid solution, 5 g of CAN, 0.1 g of $RuCl_3$ and 0.22 ml of TEOS were dissolved in 40 ml absolute ethanol. After stirring for 30 min, the resulting solution was added dropwise to 100 ml deionized water and irradiated with a high intensity ultrasonic Ti horn (20 kHz, 125 W/cm^2 at 60% efficiency) at ambient temperature for 3 h. The temperature of mixture increased to 58 °C during sonication. A similar procedure was followed for the synthesis of $Ce_{0.85}Fe_{0.1}Ru_{0.05}O_{2-\delta}$. After sonication, the product was separated by centrifugation, washed several times with ethanol and dried in hot air oven at 120 °C for 3 h.

The structure and particle size of the synthesized compounds were analyzed by XRD and TEM. X-ray diffraction (XRD) pattern of powders were recorded in a Phillips X'Pert diffractometer using a Cu Kα (λ = 1.5406 Å) radiation source at scan rate of 0.12° min^{-1} with 0.02° step size in the 2θ range between 10 and 80°. Structures were refined by the profile fitting method, using JANA 2000 program suite. Transmission electron microscopy (TEM) and high resolution transmission electron microscopy (HRTEM) images were obtained on a FEI Technai 20 operating at 200 kV. Energy dispersive X-ray microanalysis (EDX) was performed using a fine probe. A trace amount of sample was sonically dispersed in ethanol and deposited on a copper grid (300 mesh) coated with a carbon film. The electronic structure of catalyst was determined by X-ray photoelectron spectroscopy (XPS) using a Thermo Scientific Multilab 2000 instrument with Al Kα source. All the binding energies were referenced to the C (1s) peak at 284 eV and this was also verified based on the oxygen peak observed at 530 eV.

The Gaussian-Lorentzian and Shirley background was used for peak analysis. The specific surface area of the samples was measured by nitrogen adsorption at 77 K with Smartsorb 93 (Smart Instruments Company Pvt. Ltd, India). All the samples were degassed at 150 °C for 5 h prior to the measurement.

2.2. Temperature programmed reduction (H_2-TPR)

Redox behavior or OSC of both the catalysts were studied by H_2-TPR. The hydrogen uptake measurements were carried out in a quartz reactor (40 cm length and 0.4 cm of internal diameter). 25 mg of catalyst sample in powder form was loaded in the reactor and the temperature of the sample was programmed to rise at a constant rate of 10 °C/min from 30 to 450 °C in 5% H_2/Ar (Chemix, Bangalore, India) gas mixture flowing at 30 ml/min. Before the experiment, the samples were pretreated in air flow at 400 °C for 1 h in order to obtain a stable baseline. The H_2 consumption was monitored by thermal conductivity detector (TCD) and the water produced due to reduction was trapped in a molecular sieve prior to entering the TCD. The amount of H_2 uptake was calibrated against the hydrogen intake/consumption of a known weight of CuO sample.

2.3. CO oxidation and WGS activity

Catalytic activity measurements were performed in a continuous flow, fixed bed reactor at atmospheric pressure using 200 mg of catalyst (80–140 mesh) diluted with an inert glass beads. All catalysts were used in the as-synthesized form without reduction with H_2. The temperature of the catalyst bed was measured by means of a *K*-type thermocouple inserted in the middle of the bed. All reaction gases (Chemix, Bangalore India) were of ultra high purity grade. The reaction mixture consisting of 2.4 vol% of CO, 2.4 vol% of O_2 and balance with N_2 with total flow rate 100 ml/min was fed to the reactor. The gas hourly space velocity of 60,000 h^{-1} (calculated based on the catalyst bed volume of 0.1 cm^3 for 200 mg of catalyst) was kept constant for all measurements. The reaction was carried out at isothermally at several temperatures. The concentrations of CO and CO_2 in the effluent gas were analyzed on line by a gas chromatograph (Mayura Analytical, Bangalore). CO and CO_2 were separated using a Hayesep A (80–100 mesh and 3 m long) packed column and were detected using a flame ionization detector with incorporating a methanizer. The catalytic performance of the catalysts was expressed in terms of CO conversion as a function of reaction temperature. The carbon balance was always higher than 97% in each case. The utilization of lattice oxygen in the reaction was also confirmed by performing CO oxidation in the absence of fed oxygen. 1% of CO was passed along with N_2 keeping the total gas flow at 100 ml/min over 100 mg of catalyst.

WGS reaction was carried out over 300 mg of catalyst with the feed gas mixture consists of 2 vol% of CO and 98% of N_2 keeping the total gas flow rate of 100 ml/min. This corresponds to a dry space velocity of 48,000 h^{-1} (calculated based on the catalyst bed volume of 0.125 cm^3 for 300 mg of catalyst). Water was pumped using a calibrated HPLC pump in the vaporizer maintained at 160 °C and then mixed with reaction mixture before reaching the catalyst. A constant water flow of 0.05 ml/min (corresponds to 55 ml/min in vapor phase) was used for all the experiments. Therefore, the resultant composition of CO and H_2O was nearly 1.3% and 35% (on the wet basis), respectively. A steam trap was placed at the downstream of reactor to collect unreacted water and further details about the experimental setup can be found elsewhere [34].

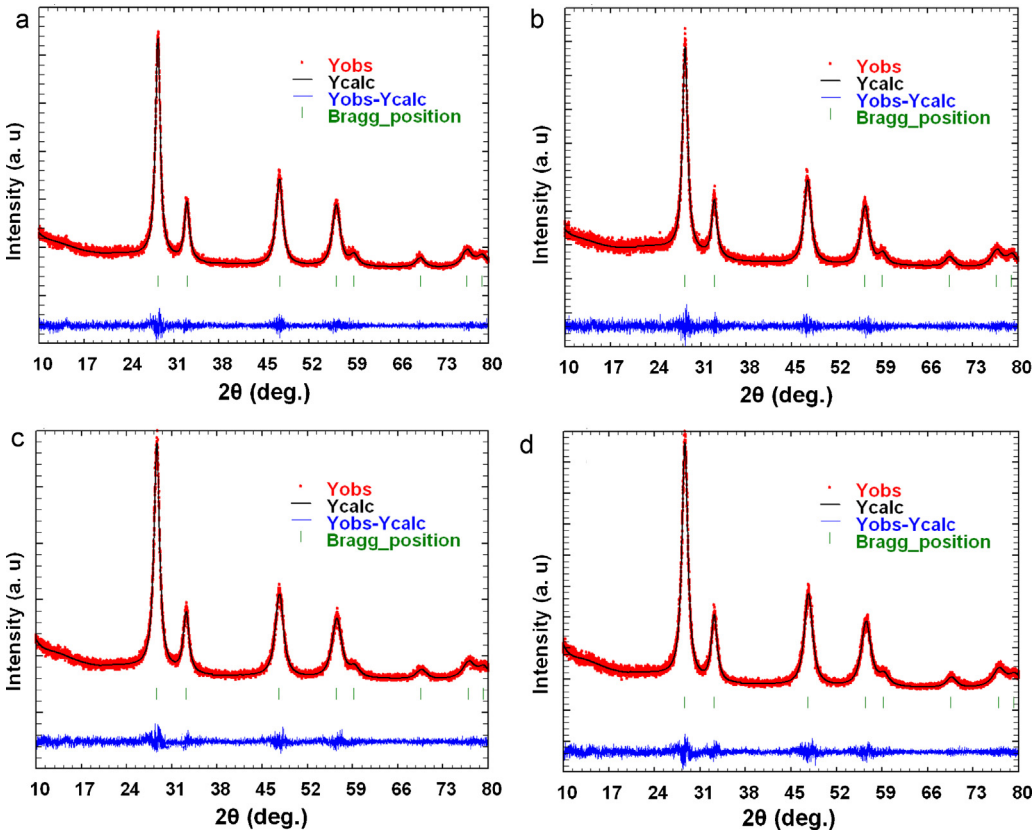

Fig. 1. Profile refined XRD patterns for $Ce_{0.85}Si_{0.1}Ru_{0.05}O_{2-\delta}$ (a) as-synthesized (b) after 3 cycles of CO oxidation, respectively, and for $Ce_{0.85}Fe_{0.1}Ru_{0.05}O_{2-\delta}$ (c) as-synthesized (d) after 3 cycles of CO oxidation, respectively.

3. Results and discussion

The solid product obtained after washing was further heated in air at 400 °C for 30 min to remove (if any) the residual of chloride/nitrates and this was termed 'as-synthesized' compound. No chloride content in the catalyst could be detected by XPS, EDX or ion chromatography. However, chloride content of lower than 100 ppm may be present in the catalyst.

3.1. Structural studies

XRD patterns of both the as-synthesized compounds are shown in Fig. 1. All the diffraction peaks can be indexed as a face centered cubic phase CeO_2 (JCPDS 34-0394) and no diffraction lines corresponding to the metal (Ru, Fe) and metal oxide (RuO_2, Fe_2O_3) were found in the diffraction patterns. The diffraction peaks corresponding to cerium silicate phases were also absent. The magnification of 20 times on y scale in the range of 30–50° does not show any indication of Ru or RuO_2. This showed the formation of single phase solid solution that can be represented by the formula $Ce_{0.85}M_{0.1}Ru_{0.05}O_{2-\delta}$ (M = Si, Fe). The XRD patterns were fitted using JANA2000 program suite. Pseudo-Voigt as peak shape function and Legendre polynomial as background function (number of terms = 15) was used for profile fitting. The observed, predicted and difference XRD patterns of both the compounds are shown in Fig. 1. Fitting of the data to the fluorite structure (space group Fm3m, no 225) gave satisfactory values of R_p and R_{wp}. The structural parameters, crystallite size and the profile fitted reliability data (R_p and R_{wp}) for both the compounds are summarized in the Table 1. A slight decrease in the lattice parameter of $Ce_{0.85}M_{0.1}Ru_{0.05}O_{2-\delta}$ (M = Si, Fe) solid solution also confirms the replacement of bigger Ce^{4+} atom by smaller metal ions (Si and Fe) in the CeO_2 lattice. The patterns show broad X-ray line width suggesting that the crystallites are nanometer in size. The average crystallite size was determined from the Scherrer formula and was found to be 16 and 14 nm, respectively, for $Ce_{0.85}Si_{0.1}Ru_{0.05}O_{2-\delta}$ and $Ce_{0.85}Fe_{0.1}Ru_{0.05}O_{2-\delta}$.

After the activity test, both the compounds were heated in the reactants mixture up to 450 °C for 10 h in 3 consecutive cycles. The XRD patterns for both the compounds after 3 cycles of CO oxidation are shown in Fig. 1. Both the compounds retained their crystal structure and no peaks corresponding to any Fe, Ru metal and metal oxide phases were detected in the XRD patterns. A slight increase in the lattice parameter of the spent $Ce_{0.85}M_{0.1}Ru_{0.05}O_{2-\delta}$ (M = Si, Fe) catalyst compared to the as-synthesized catalyst confirms partial reduction of catalysts.

Bright field and HRTEM images of $Ce_{0.85}Fe_{0.1}Ru_{0.05}O_{2-\delta}$ are shown in Fig. 2. The ring type diffraction pattern is also shown in the inset of Fig. 2(a) which can be indexed to fluorite structure

Table 1
Structural parameters for the ceria modified compounds obtained by profile refinement.

Compound	Lattice parameter (a)	R_p	R_{wp}	χ^2	Crystallite size (nm)
$Ce_{0.85}Si_{0.1}Ru_{0.05}O_{2-\delta}$ (before reaction)	5.4014	4.74	4.28	0.80	16
$Ce_{0.85}Si_{0.1}Ru_{0.05}O_{2-\delta}$ (after 3 cycles)	5.4017	4.59	4.31	0.78	17
$Ce_{0.85}Fe_{0.1}Ru_{0.05}O_{2-\delta}$ (before reaction)	5.4078	3.53	3.95	0.76	14
$Ce_{0.85}Fe_{0.1}Ru_{0.05}O_{2-\delta}$ (after 3 cycles)	5.4081	3.41	3.29	0.81	16

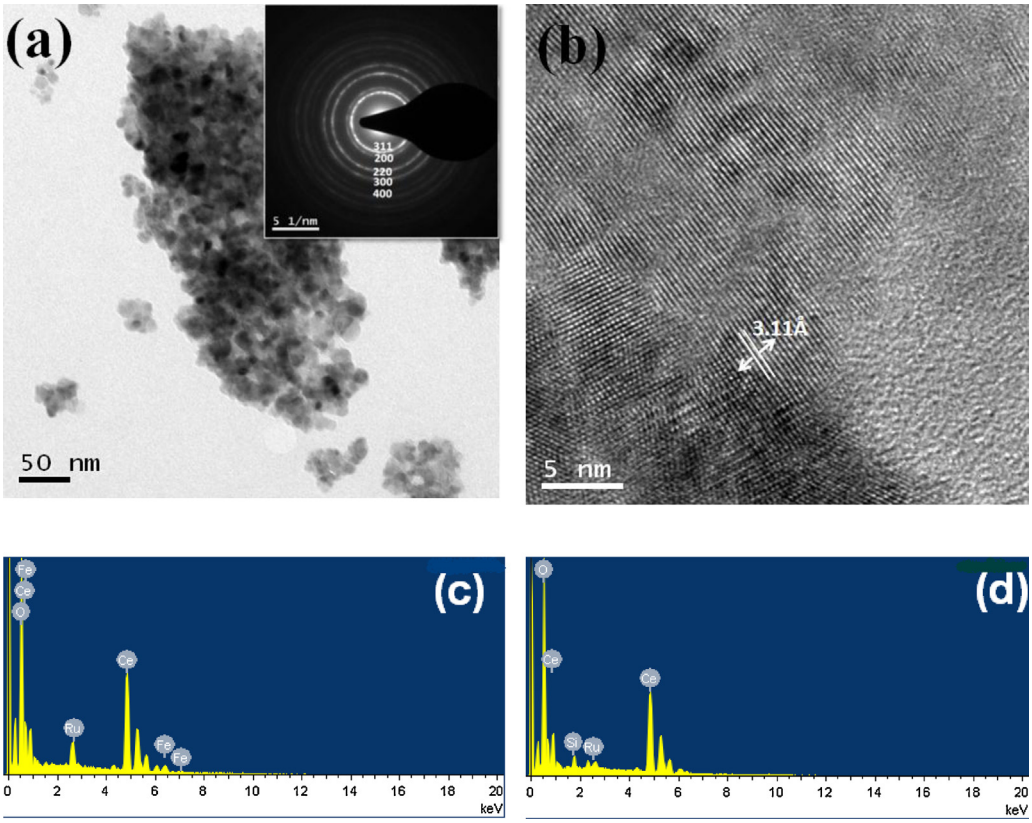

Fig. 2. (a) Bright field image, (b) HRTEM image of $Ce_{0.85}Fe_{0.1}Ru_{0.05}O_{2-\delta}$ with indexed electron diffraction in the inset of (a), (c) EDX of $Ce_{0.85}Fe_{0.1}Ru_{0.05}O_{2-\delta}$ and $Ce_{0.85}Si_{0.1}Ru_{0.05}O_{2-\delta}$, respectively.

of CeO_2. Diffraction lines corresponding to any of the metals or metal oxides (Ru and Fe) were not observed suggesting the ionic substitution of these metals in CeO_2. The bright field image shows that the particle size is 14–20 nm, which is comparable to the crystallite size determined by XRD. The spacing between two adjacent lattice planes is 3.11 Å, which corresponds to d_{111} of CeO_2 (Fig. 2(b)). EDX of both the samples is shown in Fig. 2(c) and (d), respectively, for $Ce_{0.85}Fe_{0.1}Ru_{0.05}O_{2-\delta}$ and $Ce_{0.85}Si_{0.1}Ru_{0.05}O_{2-\delta}$. The molar ratio of Ce, Ru and Fe for $Ce_{0.85}Fe_{0.1}Ru_{0.05}O_{2-\delta}$ was found to be 0.87:0.04:0.09 and the molar ratio of Ce, Ru and Si for $Ce_{0.85}Si_{0.1}Ru_{0.05}O_{2-\delta}$ was found to be 0.89:0.03:0.08. The BET surface area for $Ce_{0.85}Si_{0.1}Ru_{0.05}O_{2-\delta}$ and $Ce_{0.85}Fe_{0.1}Ru_{0.05}O_{2-\delta}$ was found to be 81 and 63 m^2/g, respectively.

XPS was used to determine the metal support interactions and possible surface processes during the reaction. The spectra were recorded both before and after the reaction. After the experiment, the reactant gases were stopped and the catalyst was cooled to room temperature in a N_2 stream. The catalyst was quickly transferred to the vacuum chamber of the spectrometer to avoid oxidation of sample. The samples were also etched in Ar stream in order to remove the surface oxide species (if any). The spent samples of the same catalyst after different reaction runs were analyzed and reproducible results were obtained.

The core level XPS of Ru (3p) in $Ce_{0.85}Si_{0.1}Ru_{0.05}O_{2-\delta}$ and $Ce_{0.85}Fe_{0.1}Ru_{0.05}O_{2-\delta}$ before and after the reaction are shown in Fig. 3. The C (1s) peak overlaps with Ru ($3d_{3/2}$) at the binding energy ~284 eV, which makes it difficult to assign the oxidation state of Ru. Therefore, the Ru (3p) spectra were examined. The binding energy of Ru (3p) in both the compounds is slightly higher (~0.3 eV) than the binding energy of Ru (462.7 eV) in RuO_2 [35]. This indicates that the chemical environment of Ru ions in both the compounds is different from that of the Ru ions in RuO_2. Ru was present mainly in the 4+ state in both the as-synthesized compounds. After the reaction, a slight shift of less than 0.3 eV towards lower binding energy was observed and this was attributed to the partial reduction of Ru^{4+}.

Fig. 4 shows the Ce (3d) spectra in the $Ce_{0.85}Si_{0.1}Ru_{0.05}O_{2-\delta}$ and $Ce_{0.85}Fe_{0.1}Ru_{0.05}O_{2-\delta}$ before and after the reaction. Six peaks

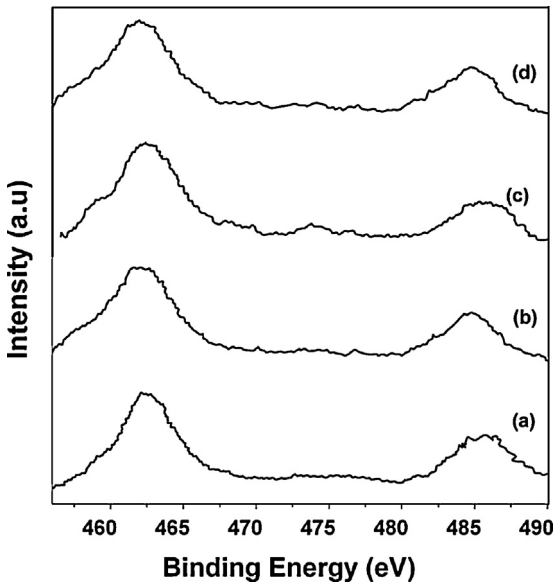

Fig. 3. Core level XPS of Ru (3p) in (a) $Ce_{0.85}Si_{0.1}Ru_{0.05}O_{2-\delta}$, before reaction (b) $Ce_{0.85}Si_{0.1}Ru_{0.05}O_{2-\delta}$, after reaction (c) $Ce_{0.85}Fe_{0.1}Ru_{0.05}O_{2-\delta}$, before reaction and (d) $Ce_{0.85}Fe_{0.1}Ru_{0.05}O_{2-\delta}$, after reaction, respectively.

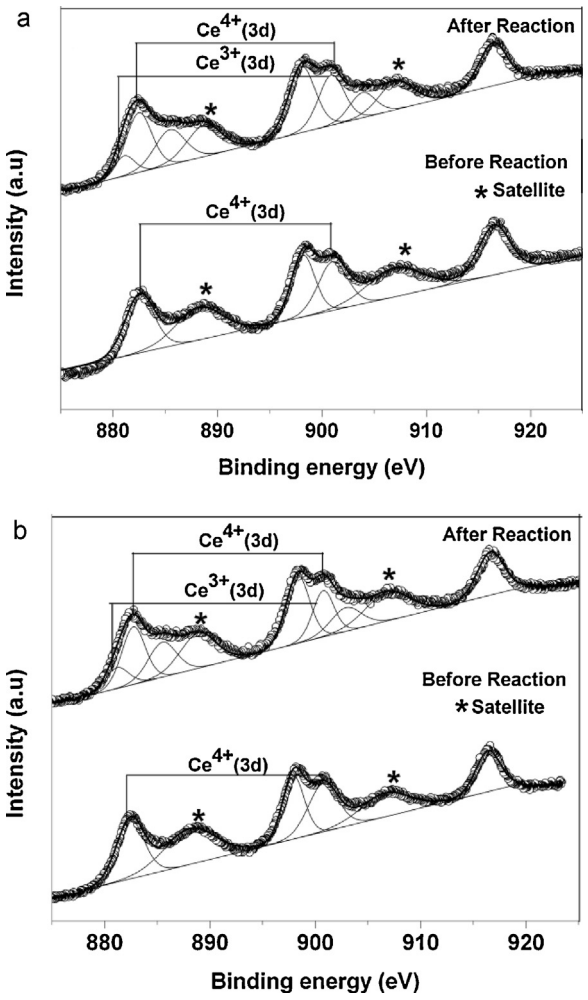

Fig. 4. Core level XPS of Ce (3d) in (a) $Ce_{0.85}Si_{0.1}Ru_{0.05}O_{2-\delta}$ and (b) $Ce_{0.85}Fe_{0.1}Ru_{0.05}O_{2-\delta}$.

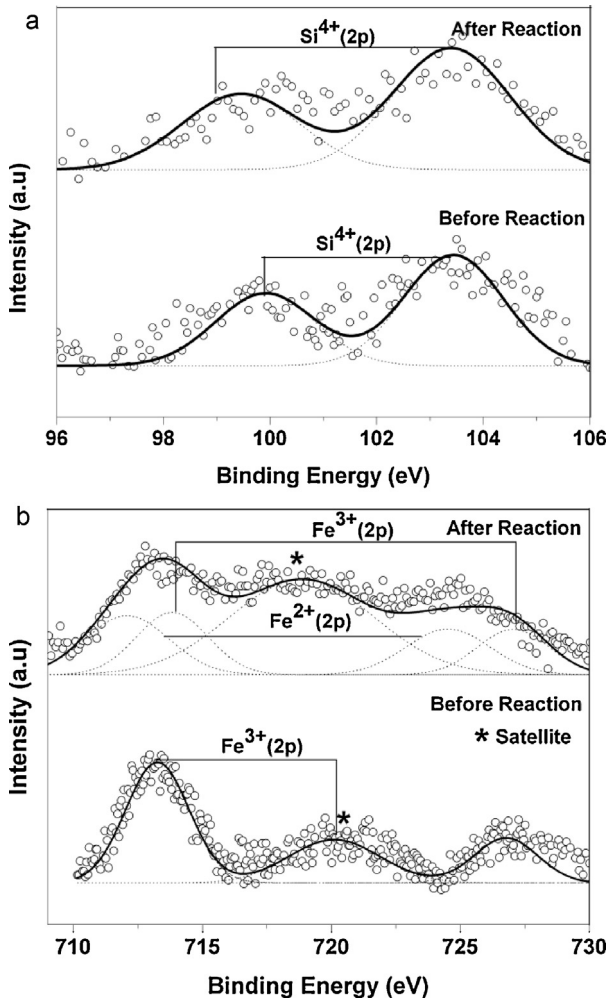

Fig. 5. Core level XPS of (a) Si (2p) in $Ce_{0.85}Si_{0.1}Ru_{0.05}O_{2-\delta}$ and (b) Fe (2p) in $Ce_{0.85}Fe_{0.1}Ru_{0.05}O_{2-\delta}$.

resulting from the pairs of spin orbit doublets were identified in CeO_2 and the peak at 882.7 eV along with its satellite peak at 889.1 eV is characteristic of Ce^{4+} in CeO_2 [36]. Therefore, Ce is mainly present in the 4+ oxidation state in both the as-synthesized compounds. After the reaction, a valley between Ce^{4+} ($3d_{5/2}$) at 882.5 eV and its satellite at 889.1 eV was partially filled indicating that Ce is present in mixed valent states (Ce^{4+} and Ce^{3+}) in both the spent catalysts [36]. Therefore, Ce (3d) spectra were deconvoluted to obtain the individual contribution of each oxidation state and the relative concentrations of Ce^{3+} in both the spent catalysts were determined. It was found be ~22% and ~27% for $Ce_{0.85}Si_{0.1}Ru_{0.05}O_{2-\delta}$ and $Ce_{0.85}Fe_{0.1}Ru_{0.05}O_{2-\delta}$, respectively. Thus, Ce^{3+} induces the formation of oxygen vacancies in the material, which are essential for absorption/dissociation of oxygen molecules during the reaction.

Fig. 5(a) shows the Si (2p) spectra in the $Ce_{0.85}Si_{0}.1Ru_{0.05}O_{2-\delta}$ catalyst before and after the reaction. The binding energy of Si ($2p_{1/2}$) is at 103 eV and can be assigned to Si^{4+} state [37]. After the reaction, there was no change in the spectra indicating no reduction of Si occurred during the reaction. The core level Fe (2p) spectra in $Ce_{0.85}Fe_{0.1}Ru_{0.05}O_{2-\delta}$ before and after the reaction are shown in Fig. 5(b) Fe is mainly present in the 3+ oxidation state in the as-synthesized compound [38]. However, the XPS spectra after the reaction showed a broad peak compared to as-synthesized catalyst suggesting the presence of mixed Fe^{3+}/Fe^{2+} species. Therefore, the XPS results show that the formation of the oxygen defects is the primary reason for high catalytic activity at low temperatures.

3.2. H_2-TPR

The oxygen storage capacity (OSC) and reducibility of catalyst are the key parameters for low temperature CO oxidation. Therefore, H_2-TPR was used to characterize the oxygen reducibility of modified CeO_2. The H_2 uptake profiles for ceria modified compounds are shown in Fig. 6. The compound containing only Ru exhibits broad reduction peaks centered around 190 °C and 370°, respectively. A low temperature peak is attributed to the reduction of ruthenium oxide species and a high temperature peak is assigned to the reduction of CeO_2 through hydrogen spillover from Ru species [39]. The addition of Si- and Fe- to $Ce_{0.95}Ru_{0.05}O_{2-\delta}$ not only lowers the reduction temperature (~140 °C) of ruthenium oxide but also increases the reducibility (H_2 consumption) of both the catalysts. The increase in the reducibility of $Ce_{0.95}Ru_{0.05}O_{2-\delta}$ on the substitution of Si- and Fe- indicates that synergistic interaction exists among the Ru and Si/Fe and CeO_2 support.

Due to the irreducible nature of Si, a much higher degree of reduction was observed for $Ce_{0.85}Si_{0.1}Ru_{0.05}O_{2-\delta}$ in comparison with $Ce_{0.85}Fe_{0.1}Ru_{0.05}O_{2-\delta}$ catalyst. The reduction of Fe^{3+} species in $Ce_{0.9}Fe_{0.1}O_{2-\delta}$ occurs at ~400 °C. However, a single hydrogen uptake peak at ~140° C was observed for $Ce_{0.85}Fe_{0.1}Ru_{0.05}O_{2-\delta}$;

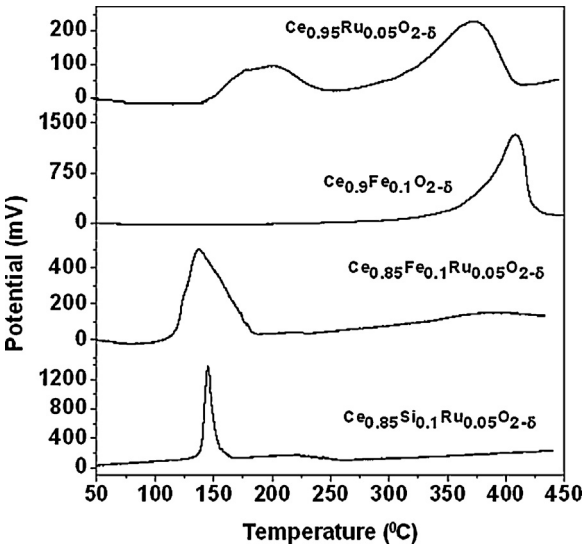

Fig. 6. H_2-TPR profile for various ceria modified compounds.

Therefore, the absence of the separate reduction peak at 400 ° C clearly indicates Fe^{3+} ions are also reduced along with Ru^{4+} ions in $Ce_{0.85}Fe_{0.1}Ru_{0.05}O_{2-\delta}$. It indicates that ionic substitution of Ru^{4+} in $Ce_{0.85}Fe_{0.1}Ru_{0.05}O_{2-\delta}$ facilitates reduction at a lower temperature. If only Ru^{4+} was reduced to the Ru_0 state, the H_2/Ru ratio should be 2. However, this ratio was found to be 4.9 and 4.11, respectively, for $Ce_{0.85}Si_{0.1}Ru_{0.05}O_{2-\delta}$ and $Ce_{0.85}Fe_{0.1}Ru_{0.05}O_{2-\delta}$ (≤250 °C), which indicates a hydrogen spillover from Ru^{4+} ions to neighboring Ce^{4+} ions. The H_2/Ru ratio for $Ce_{0.95}Ru_{0.05}O_{2-\delta}$ was found to be ∼2.1 which means that Ru^{4+} entirely reduced to Ru0 (metal). Therefore, the enhancement in the CO activity for both Si- and Fe- modified Ru/ceria catalysts is mainly due to the increase in the utilization of lattice oxygen by CO at low temperature, which is subsequently rejuvenated by oxygen molecules.

3.3. Cyclic oxygen storage behavior

H_2-TPR profile was used to study the cyclic redox behavior of both the ceria modified compounds and the correlation between OSC and catalytic activity was investigated. OSC measurements were performed repeatedly by reducing the catalyst in 5% H_2/Ar up to 450 followed by re-oxidation in air at 200 °C. The area under H_2-TPR profile was used to calculate the OSC and the histogram corresponding OSC of three successive cycles are shown in Fig. 7. OSC up to 250 °C for first (C_1), second (C_2) and third (C_3) cycle is 1570, 706 and 566 μmol/g, respectively for $Ce_{0.85}Si_{0.1}Ru_{0.05}O_{2-\delta}$ and 1295, 1143 and 1055 μmol/g, respectively, for $Ce_{0.85}Fe_{0.1}Ru_{0.05}O_{2-\delta}$. After the first H_2-TPR cycle (C_1), some loss in OSC was observed in subsequent cycles indicating some irreversible change occurred over the catalyst surface. A large irreversible surface change was observed for $Ce_{0.85}Si_{0.1}Ru_{0.05}O_{2-\delta}$ compared to $Ce_{0.85}Fe_{0.1}Ru_{0.05}O_{2-\delta}$. The dopants with lower ionic radii than the Ce cation tend to weaken the bonds of the oxygen atoms to the surface and increase reactivity of oxygen during the reduction process. The present H_2-TPR results show that OSC of $Ce_{0.85}Si_{0.1}Ru_{0.05}O_{2-\delta}$ is higher in first redox cycle indicating that the extent of lattice distortions is higher in $Ce_{0.85}Si_{0.1}Ru_{0.05}O_{2-\delta}$ compared to $Ce_{0.85}Fe_{0.1}Ru_{0.05}O_{2-\delta}$. Further, Si is irreducible and Fe is reducible which makes Fe to adapt different oxidation states during redox treatment. The presence of this additional redox cycle is responsible for good OSC of $Ce_{0.85}Fe_{0.1}Ru_{0.05}O_{2-\delta}$ during subsequent redox cycles. In addition to this, the substitution of Si makes the surface oxygen atoms more reactive in comparison with Fe. Therefore, $Ce_{0.85}Si_{0.1}Ru_{0.05}O_{2-\delta}$ is a good oxidant rather than a good oxidation catalyst. The lattice oxygen is easily consumed by the H_2 with the formation of oxygen vacancies; however these vacancies are not filled rapidly by gas phase oxygen. Despite this, both the catalysts manifested reasonably good reversibility in redox environment. The OSC of $Ce_{0.95}Ru_{0.05}O_{2-\delta}$ was found to be 305 μmol/g, which is much lower that the present catalysts. The H_2 consumption or OSC of the catalyst was calculated base on area under the curve. The TCD signal (mV) is also given in the Fig. 6 to avoid confusion. The TCD signal (*y*-axis) in $Ce_{0.85}Fe_{0.1}Ru_{0.05}O_{2-\delta}$ is nearly six times higher than $Ce_{0.95}Ru_{0.05}O_{2-\delta}$. Therefore, $Ce_{0.85}Fe_{0.1}Ru_{0.05}O_{2-\delta}$ represents higher OSC than $Ce_{0.95}Ru_{0.05}O_{2-\delta}$. Therefore, the addition of Si- and Fe in $Ce_{0.95}Ru_{0.05}O_{2-\delta}$ facilitates surface oxygen reduction and the increases in OSC of both catalysts can be attributed to the enhancement in the catalytic activity.

3.4. CO oxidation activity and kinetic study

Having studied the cyclic redox behavior by H_2-TPR, the application of these high OSC compounds were explored in exhaust catalysis. CO oxidation was carried out with these catalysts both in the presence and absence of feed O_2 and % CO conversion over both the catalysts is shown in Fig. 8. In the presence of feed O_2, nearly complete conversion (∼99%) of CO was achieved below 200 °C with both the catalysts. CO oxidation reaction was also carried out over $Ce_{0.95}Ru_{0.05}O_{2-\delta}$ prepared by sonication method and the activity was compared with $Ce_{0.85}M_{0.1}Ru_{0.05}O_{2-\delta}$ (M = Si, Fe). It is found that the activity of both the $Ce_{0.85}M_{0.1}Ru_{0.05}O_{2-\delta}$ (M = Si, Fe) catalysts is several fold higher than $Ce_{0.95}Ru_{0.05}O_{2-\delta}$. The considerable enhancement in the activity is attributed the greater reducibility of $Ce_{0.85}M_{0.1}Ru_{0.05}O_{2-\delta}$ (M = Si, Fe) as evident from H_2-TPR study. Nearly 97% of CO conversion was observed up to 320 °C even in the absence of feed O_2 and this suggests that the lattice oxygen is activated in both the catalysts for CO oxidation. It is also clear from Fig. 6 that the higher utilization of lattice oxygen was observed in $Ce_{0.85}Si_{0.1}Ru_{0.05}O_{2-\delta}$ compared to $Ce_{0.85}Fe_{0.1}Ru_{0.05}O_{2-\delta}$ and these results are consistent with our H_2-TPR results.

The rate of reaction and activation energy of the catalysts for CO oxidation reaction were determined by performing the reaction with different weights of the catalyst keeping the total gas flow

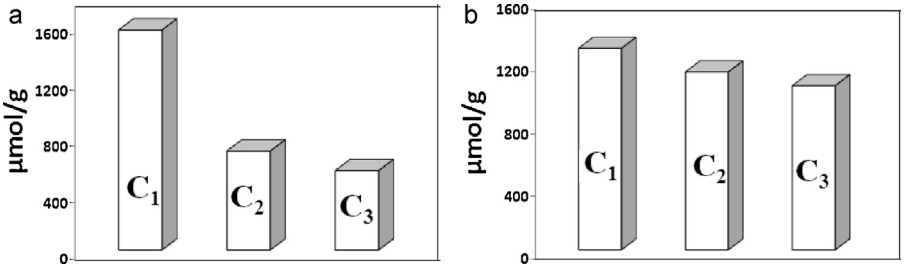

Fig. 7. OSC of (a) $Ce_{0.85}Si_{0.1}Ru_{0.05}O_{2-\delta}$ and (b) $Ce_{0.85}Fe_{0.1}Ru_{0.05}O_{2-\delta}$ after three consecutive reduction cycles.

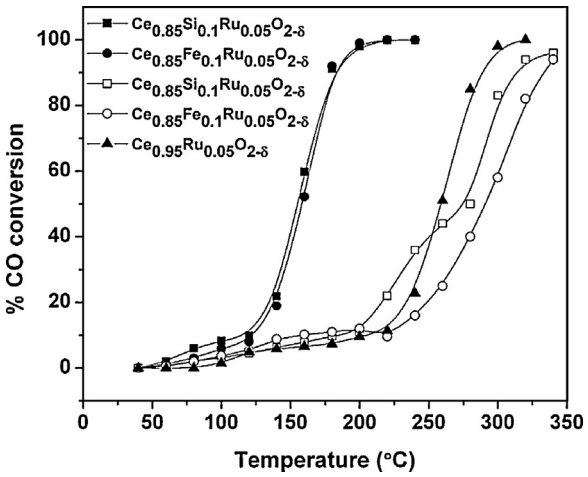

Fig. 8. Variation of CO conversion with temperature over various ceria modified catalysts.

and GHSV same. The rate of reaction was used to calculate from the following.

$$\text{Rate}(r) = \frac{F \times x}{W} = \frac{x}{W/F} \quad (1)$$

where F is the flow of the gas in mol/s, W is the weight of the catalyst in g and x is the fractional CO conversion. The plot of fractional CO conversion with W/F at various temperatures is shown in Fig. 9(a) and (b), for $Ce_{0.85}Si_{0.1}Ru_{0.05}O_{2-\delta}$ and $Ce_{0.85}Fe_{0.1}Ru_{0.05}O_{2-\delta}$ catalysts, respectively. The plot is linear up to 30% conversion and the reaction rate was determined from the slope of linear portion. The variation of rate of reaction with temperature is shown in Fig. 9(c) and (d), respectively, for $Ce_{0.85}Si_{0.1}Ru_{0.05}O_{2-\delta}$ and $Ce_{0.85}Fe_{0.1}Ru_{0.05}O_{2-\delta}$. The apparent activation energy of the CO oxidation reaction was calculated from the Arrhenius plot (inset of Fig. 9(c) and (d)) and found to be 39 kJ/mol for $Ce_{0.85}Si_{0.1}Ru_{0.05}O_{2-\delta}$ and 44 kJ/mol for $Ce_{0.85}Fe_{0.1}Ru_{0.05}O_{2-\delta}$ respectively. The comparison of reaction rate and activation energy of various catalysts examined in previous studies [40–47] is given in Table 2. The present catalysts are superior in terms of the high rate of reaction and low activation energy. Therefore, both the catalysts are promising candidates for low temperature CO oxidation.

The effect of concentration of CO and O_2 on the rate of reaction was studied under isothermal conditions with a differential reactor approach. The rates of reaction were measured for both the catalysts by keeping one reactant concentration constant and varying the other concentration of the other reactant. The concentration of CO was varied between 1 and 3%, keeping the concentration of O_2 constant at 2.4% and the composition of O_2 was changed from 0.5 to 3%, keeping the concentration of CO constant at 2.4% (all in volume basis). The total gas flow rate and catalyst loading were kept constant at 100 cm^3/min and 100 mg, respectively. Fig. 10 shows the dependence of reaction rate on the partial pressure of CO and O_2 at different temperatures for $Ce_{0.85}Si_{0.1}Ru_{0.05}O_{2-\delta}$ and $Ce_{0.85}Fe_{0.1}Ru_{0.05}O_{2-\delta}$. At low concentration, the rate of reaction rapidly increases with CO and O_2 concentration and saturates at high concentration of CO and O_2 for both the catalysts. The rates with CO and CO_2 were plotted as a function of temperature and apparent reaction order was obtained from the slope of the curve. At low concentration of O_2, the reaction has a positive order in O_2 and order of reaction changes to zero at higher concentration of O_2 for both the catalysts. At low concentration of CO, the dependence is approximately first order in CO for both the catalysts. If either concentrations of CO or O_2 were varied, no maximum in the reaction rate was observed. This indicates that CO and O_2 do not adsorb competitively on the surface of catalyst. This information was used while deriving the kinetic model.

3.5. Kinetic model

The identity and reducibility of the support have a great influence on the catalytic performance. Reducible supports such as CeO_2, TiO_2, Fe_2O_3 often exhibits higher activity at low temperature as compared to non-reducible supports like Al_2O_3, SiO_2 [44,48,49]. The reducibility of support also plays an important role in the stabilization of various intermediate species and renders different reaction pathways [50,51]. Therefore, mono functional Langmuir–Hinshelwood (L–H) type reaction mechanism has been proposed for non-reducible supports and bifunctional redox mechanism is considered to be operative over reducible supports [52,53]. The bifunctional redox mechanism is a special case of the noncompetitive L–H mechanism in which CO is adsorbed on the noble metal site and activation of O_2 takes place on the support. The role of reducible oxides is not limited to weaken the CO adsorption on the active sites (noble metals) but also provide additional sites for adsorption/activation of O_2 [54]. Therefore, the noble metals supported over reducible oxides show high activities for CO oxidation reaction due to change in the competitive L–H mechanism to a noncompetitive dual site L–H mechanism. Previously, we have proposed several plausible mechanisms for CO oxidation over $Ti_{0.99}Pd_{0.01}O_{1.99}$ and it was found that the contribution from the mono functional mechanism to the overall rate of CO_2 formation was negligible and bifunctional redox mechanism is dominant [44]. Mars van Krevelen mechanism (also called the redox mechanism) was proposed mainly for Cu based catalysts, which involves reduction of catalyst surface by CO and reoxidation of catalyst surface with O_2 [55]. Recently, the application of the temporal analysis of products reactor measurements was used to investigate the CO oxidation over gold catalysts and a gold assisted Mars-van Krevelen mechanism was proposed [10,56]. However, the derivation of Mars-van Krevelen mechanism has a number of assumptions;

Table 2
Reaction rates and activation energies for the CO oxidation reaction on various catalysts.

Catalyst	Rate (μmol/g/s) (°C)	Activation energy (kJ/mol)	Reference
5 wt% Pd/SiO_2	0.316(143)	103	[40]
$Pd/CeO_2/Al_2O_3$	38(250)	84	[41]
0.5 wt% $Pd/CeO_2/Al_2O_3$	0.7(220)	175	[42]
Pt/Al_2O_3	0.05(130)	115	[43]
Pd/Al_2O_3	1.8(135)	74	[43]
$Ti_{0.99}Pd_{0.01}O_{2-\delta}$	13.83(120)	53.13	[44]
$Ce_{0.98}Pd_{0.02}O_{2-\delta}$	3.9(120)	121	[45]
0.014 wt Rh/9 wt % Ce/Al_2O_3	0.95(196)	90.3	[46]
$Ce_{0.73}Ti_{0.25}Pd_{0.02}O_{2-\delta}$	–	53.5	[47]
5 wt % Pt/SiO_2	0.32(115)	56	[40]
$Ce_{0.85}Si_{0.1}Ru_{0.05}O_{2-\delta}$	2(140)	39	(Present study)
$Ce_{0.85}Fe_{0.1}Ru_{0.05}O_{2-\delta}$	1.69(140)	44	(Present study)

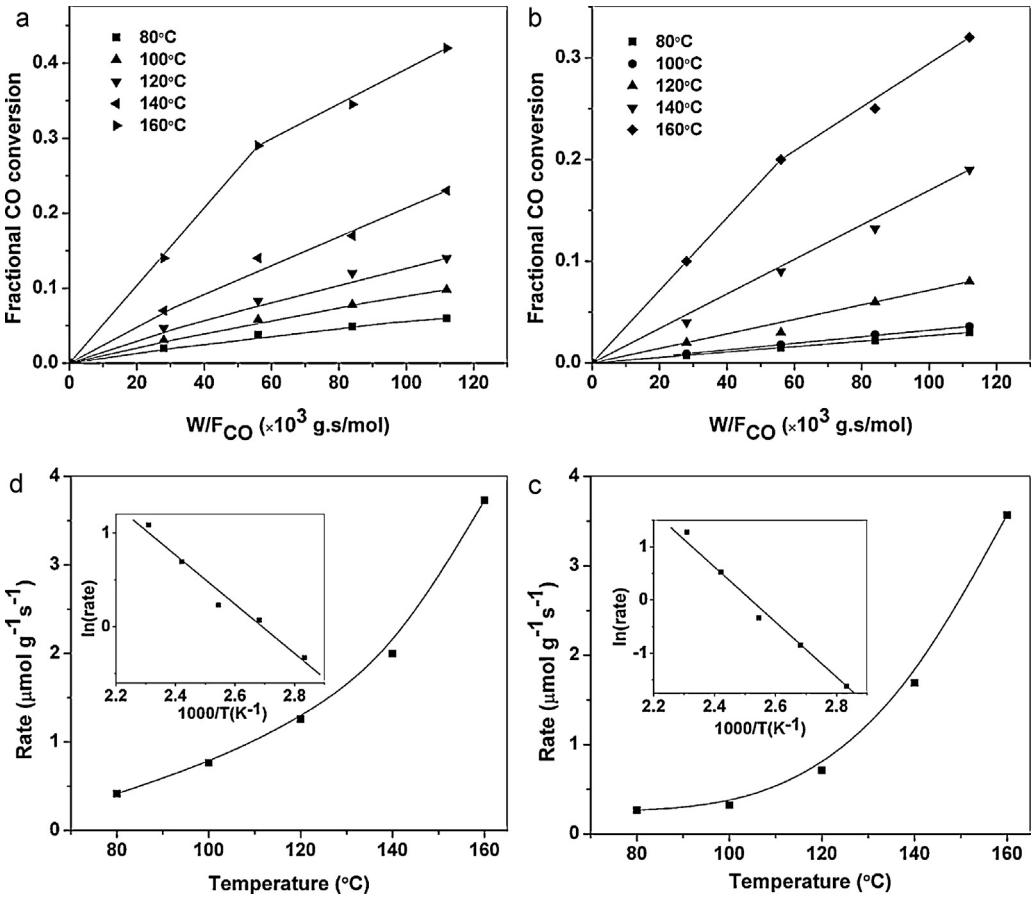

Fig. 9. Variation of fractional conversion of CO with W/F_{CO} for (a) $Ce_{0.85}Si_{0.1}Ru_{0.05}O_{2-\delta}$ (b) $Ce_{0.85}Fe_{0.1}Ru_{0.05}O_{2-\delta}$ and rate of reaction as function of temperature for (c) $Ce_{0.85}Si_{0.1}Ru_{0.05}O_{2-\delta}$ (d) $Ce_{0.85}Fe_{0.1}Ru_{0.05}O_{2-\delta}$ for CO oxidation.

therefore this expression must be used as a mathematical data-fitting function [57]. Further, the applicability of this expression is limited only for reactions involving molecularly adsorbed oxygen species on a single site and cannot be used for reaction involving utilization of the lattice oxygen [57]. The present study also emphasizes the direct relation between ceria reducibility and CO conversion and an increase in ceria reducibility improves the density of active sites (vacancies).

Based on experimental results and above discussion, a possible set of elementary steps were proposed. The reaction mechanisms are essentially a bifunctional redox kind mechanism, which involves adsorption of CO over the catalyst followed by oxidation by extraction of lattice oxygen, and rejuvenation of oxide vacancies by feed O_2 to complete catalytic cycle. Various possible steps involved in the mechanism can be written as

$$CO + M \overset{K_1}{\longleftrightarrow} CO - M \quad (2)$$

$$CO - M + Ce^{4+} \overset{k_2}{\longrightarrow} CO_2 + M + Ce^{3+\square} \quad (3)$$

$$O_2 + Ce^{3+\square} \overset{k_3}{\longrightarrow} Ce^{4+} \quad (4)$$

M, Ce^{4+} and $Ce^{3+\square}$ represent metal cation (Ru and Fe), oxidized catalyst and vacancy on support, respectively. Eq. (2) depicts the adsorption/desorption equilibrium of CO and Eq. (3) shows the subsequent extraction of lattice oxygen from the ceria surface by CO to form a intermediate, which decomposes to release CO_2 with the creation of oxygen vacancies. Our H_2-TPR and XPS studies revealed that the surface Ce–O is substantially weakened on the substitution of metal cation cations (Ru, Si, Fe) in CeO_2 matrix and facilitated the formation of more reducible oxygen at low temperature. CO oxidation in the absence of the feed O_2 also corroborates that the utilization of lattice oxygen is possible during reaction. The gas phase oxygen will fill the oxygen vacancies (Eq. (4)) for completion of catalyst cycle. Therefore, the gas phase oxygen oxidizes the reduced ceria support and metal cation facilitates the oxygen ion mobility and reducibility of support apart from providing CO adsorption sites. While deriving the rate expression, it is implicitly assumed that the reaction takes place at the interface of metal sites and support. The rate expression obtained after solving the above set of elementary steps is

$$r_{CO_2} = \frac{K_1 k_2 k_3 C_{CO} C_{O_2}}{K_1 k_2 C_{CO} + k_3 C_{O_2}(1 + K_1 C_{CO})} \quad (5)$$

Eq. (5) can be rewritten as

$$\frac{1}{r_{CO_2}} = \frac{1}{k_3 C_{O_2}} + \frac{1 + K_1 C_{CO}}{K_1 k_2 C_{CO}} \quad (6)$$

By varying C_{CO} at constant C_{O_2} and varying C_{O_2} at constant C_{O_2}, the values of the individual rate constants were determined. These values were used as initial guesses and the initial guesses for K_1, k_2 and k_3 were used for regression. The experimentally observed rates were fitted against the calculated rate and kinetic parameters were optimized using non-linear regression technique based on Levenberg–Marquardt algorithm. The optimized kinetic parameters for both the catalysts are given in Table 4. Comparison between experimentally observed rate and calculated rate from the model for the both the catalysts are shown in Fig. 11.

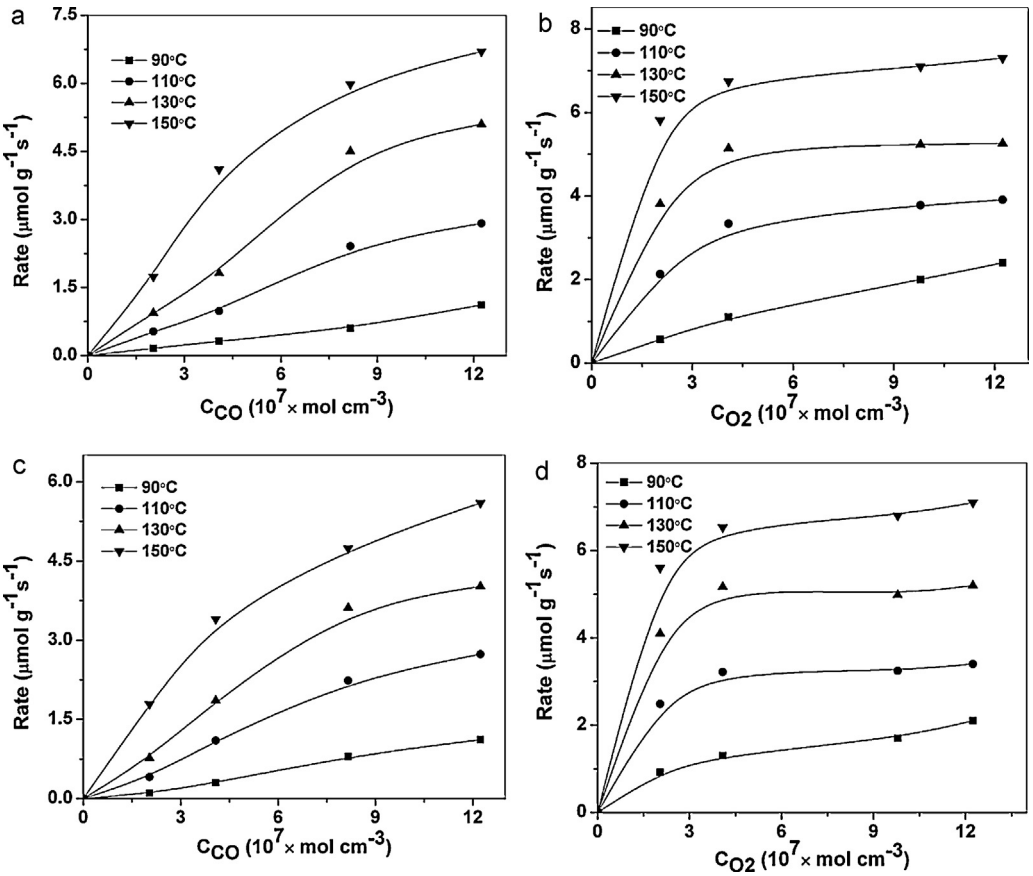

Fig. 10. (a) The effect of partial pressure of CO on the formation of CO_2 at a constant $C_{O_2} = 9.8 \times 10^{-7}$ mol/cm^3 and (b) effect of O_2 partial pressure on the formation of CO_2 at a constant $C_{CO} = 9.8 \times 10^{-7}$ mol/cm^3, respectively, with $Ce_{0.85}Si_{0.1}Ru_{0.05}O_{2-\delta}$ and (c) the effect of partial pressure of CO on the formation of CO_2 at a constant $C_{O_2} = 9.8 \times 10^{-7}$ mol/cm^3 and (d) effect of O_2 partial pressure on the formation of CO_2 at a constant $C_{CO} = 9.8 \times 10^{-7}$ mol/cm^3, respectively, with $Ce_{0.85}Fe_{0.1}Ru_{0.05}O_{2-\delta}$.

3.6. WGS activity

Having established high activity of both the compounds for low temperature CO oxidation, the performance of these compounds was also investigated for WGS reaction. Fig. 11 shows the steady state concentrations of CO, CO_2 and H_2 as a function of temperature for both the ceria modified compounds. The concentrations depicted in Fig. 12 were normalized by the initial concentration of CO. Nearly complete CO conversion (~99%) was observed at 280 °C and 300 °C for $Ce_{0.85}Si_{0.1}Ru_{0.05}O_{2-\delta}$ and $Ce_{0.85}Fe_{0.1}Ru_{0.05}O_{2-\delta}$, respectively. The equilibrium conversion

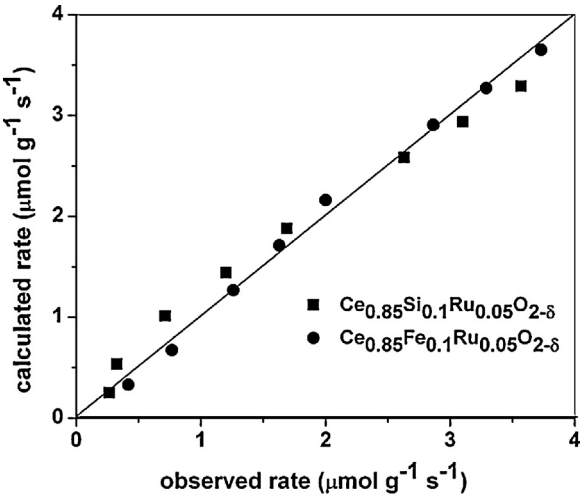

Fig. 11. Comparison between experimentally measured rate and calculated rate from the model.

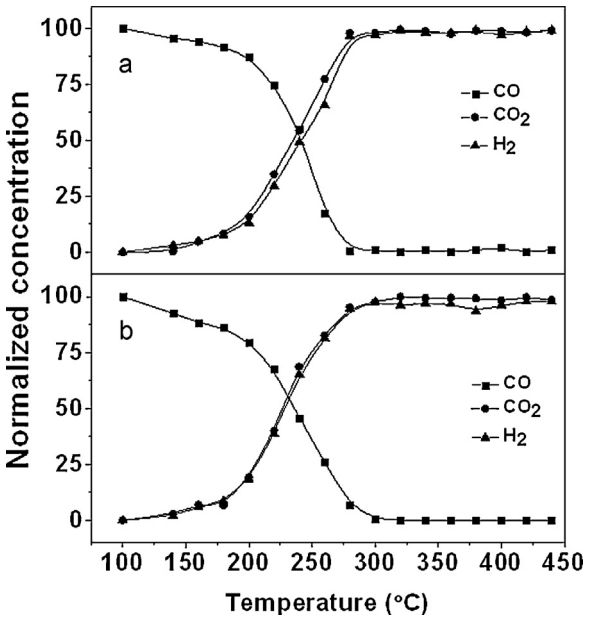

Fig. 12. Normalized CO, CO_2 and H_2 concentrations in WGS reaction over the (a) $Ce_{0.85}Si_{0.1}Ru_{0.05}O_{2-\delta}$ and (b) $Ce_{0.85}Fe_{0.1}Ru_{0.05}O_{2-\delta}$, respectively.

Table 3
Reaction rates and activation energies for the WGS reaction on various catalysts.

Catalyst	Rate (μmol/g/s) (°C)	Activation energy (kJ/mol)	Reference
1.5%Pt10%La/CeO_2	1(350)	75.31	[61]
2.7%Pt10%La/CeO_2	1.5(350)	75.31	[61]
3.7%Pt10%La/CeO_2	2(350)	75.31	[61]
$Ce_{0.78}Ti_{0.2}Pt_{0.02}O_{2-\delta}$	7.54(280)	56.48	[62]
$Ce_{0.98}Pt_{0.02}O_{2-\delta}$	4.5(220)	52	[62]
$Ce_{0.65}Fe_{0.33}Pt_{0.02}O_{2-\delta}$	4.05(275)	50.62	[63]
$Ce_{0.98}Pt_{0.02}O_{2-\delta}$	6.62(280)	62.76	[64]
$Ti_{0.84}Pt_{0.01}Fe_{0.15}O_{2-\delta}$	2.74(280)	63	[65]
Pd/Al_2O_3	0.18(180)	65	[66]
Pd/CeO_2	1.5(225–275)	38	[67]
Ru/CeO_2	0.01(700)	–	[68]
$Ce_{0.85}Si_{0.1}Ru_{0.05}O_{2-\delta}$	1.64(220)	51	Present study
$Ce_{0.85}Fe_{0.1}Ru_{0.05}O_{2-\delta}$	1.4(220)	56	Present study

based on the mentioned flow rate can be calculated [58] and this is found be 99%. $Ce_{0.85}Si_{0.1}Ru_{0.05}O_{2-\delta}$ showed higher reactivity than $Ce_{0.85}Fe_{0.1}Ru_{0.05}O_{2-\delta}$ and is consistent with the reported OSC data. The possible byproducts of the reaction such as methane and other hydrocarbons were not detected in the product stream within the detection limit of 5 ppm and both the catalysts are 100% selective towards the hydrogen production. A lack of methanation activity is an important finding of the present study and this may be attributed to the ionic substitution of Ru metal. Ru metal is well known for CO methanation and Fischer Tropsch activity [59,60]. The comparison of reaction rate and activation energy various catalysts examined in previous studies is given in Table 3. Therefore, the present compounds are highly active and selective for WGS reaction.

WGS reaction was performed with different weights of the catalysts, keeping the total flow rate and GSHV constant.

Table 4
Optimized rate parameters for CO oxidation reaction over $Ce_{0.85}Si_{0.1}Ru_{0.05}O_{2-\delta}$ and $Ce_{0.85}Fe_{0.1}Ru_{0.05}O_{2-\delta}$.

Parameter	$Ce_{0.85}Si_{0.1}Ru_{0.05}O_{2-\delta}$	$Ce_{0.85}Fe_{0.1}Ru_{0.05}O_{2-\delta}$
K_1	$165\sqrt{T}\exp(2432/T)$	$149\sqrt{T}\exp(2552/T)$
k_2	$4.4\times10^4\sqrt{T}$	$2.7\times10^4\sqrt{T}$
k_3	$1.5\times10^4\exp(-4587/T)$	$2.9\times10^4\exp(-4927/T)$

Fig. 13(a) and (b) shows the variation of W/F_{CO} with the fractional conversion of CO, respectively, for $Ce_{0.85}Si_{0.1}Ru_{0.05}O_{2-\delta}$ and $Ce_{0.85}Fe_{0.1}Ru_{0.05}O_{2-\delta}$. The rates of WGS reaction at various temperatures were calculated from the slope of the curve and are shown in Fig. 13(c) and (d), respectively, for $Ce_{0.85}Si_{0.1}Ru_{0.05}O_{2-\delta}$ and $Ce_{0.85}Fe_{0.1}Ru_{0.05}O_{2-\delta}$. The activation energy was calculated from Arrhenius plots (in the inset of Fig. 13(c) and (d)) and found to be

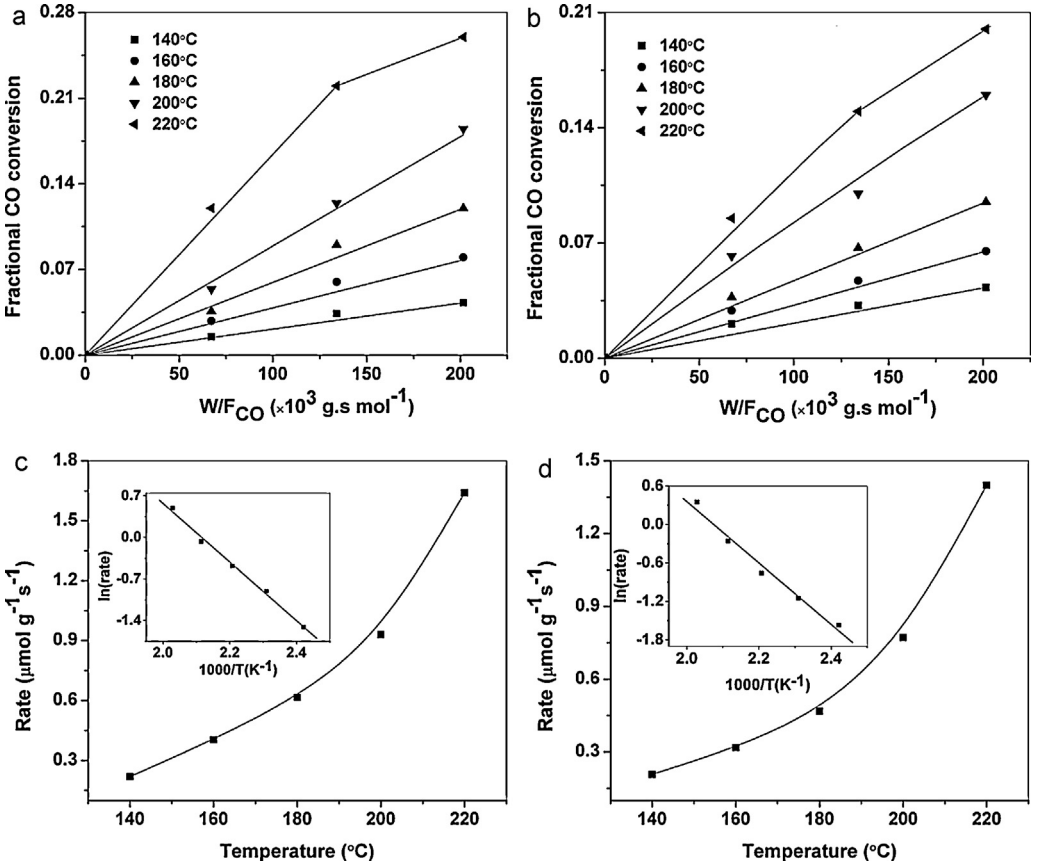

Fig. 13. Variation of fractional conversion of CO with W/F_{CO} for (a) $Ce_{0.85}Si_{0.1}Ru_{0.05}O_{2-\delta}$ (b) $Ce_{0.85}Fe_{0.1}Ru_{0.05}O_{2-\delta}$ and rate of reaction as function of temperature for (c) $Ce_{0.85}Si_{0.1}Ru_{0.05}O_{2-\delta}$ (d) $Ce_{0.85}Fe_{0.1}Ru_{0.05}O_{2-\delta}$ for WGS reaction.

51 kJ/mol and 56 kJ/mol, respectively, for $Ce_{0.85}Si_{0.1}Ru_{0.05}O_{2-\delta}$ and $Ce_{0.85}Fe_{0.1}Ru_{0.05}O_{2-\delta}$. In summary, this study demonstrates that both $Ce_{0.85}Si_{0.1}Ru_{0.05}O_{2-\delta}$ and $Ce_{0.85}Fe_{0.1}Ru_{0.05}O_{2-\delta}$ are not only good OSC materials but also good catalysts for energy and environmental applications.

4. Conclusions

The activity of $Ce_{0.95}Ru_{0.05}O_{2-\delta}$ for CO oxidation and water gas shift reaction was greatly enhanced on the addition of Si- and Fe and the largest effect was manifested by Si. The increase in the activity directly correlated with enhanced in the reducibility of ceria. Both the ceria modified compounds are reversible in cyclic redox conditions and therefore, potential candidates for energy and environmental applications. Further, a lack of methanation activity is also an important finding of the present study and this may be attributed to the ionic substitution of Ru metal. The high catalytic activity exhibited by the present catalysts for CO oxidation and WGS reaction is encouraging and might be alternative for highly expensive Au, Pt, Pd and Rh catalysts. The understanding of structure, surface process, and catalytic behavior of the present materials also provide some guidelines for the design of efficient and cost effective catalyst for CO oxidation.

Acknowledgment

The authors thank Department of Science and Technology, Govt. of India for financial support.

References

[1] F. Esch, S. Fabris, L. Zhou, T. Montini, C. Africh, P. Fornasiero, G. Comelli, R. Rosei, Science 309 (2005) 752–755.
[2] T. Baidya, A. Gupta, P.A. Deshpandey, G. Madras, M.S. Hegde, Journal of Physical Chemistry C 113 (2009) 4059–4068.
[3] H. Yao, Y.F. Yao, Journal of Catalysis 86 (1984) 254–265.
[4] R. Di Monte, J. Kašpar, H. Bradshaw, C. Norman, Journal of Rare Earths 26 (2008) 136–140.
[5] S.Y. Christou, J. Gåsste, H.L. Karlsson, J.L.G. Fierro, A.M. Efstathiou, Topics in Catalysis 52 (2009) 2029–2034.
[6] S.Y. Christou, S. García-Rodríguez, J.L.G. Fierro, A.M. Efstathiou, Applied Catalysis B: Environmental 111–112 (2012) 233–245.
[7] C.M. Kalamaras, I.D. Gonzalez, R.M. Navarro, J.G. Fierro, A.M. Efstathiou, Journal of Physical Chemistry C 115 (2011) 11595–11610.
[8] L. Kundakovic, M. Flytzani-Stephanopoulos, Journal of Catalysis 179 (1998) 203–221.
[9] D.A. Constantinou, A.M. Efstathiou, Applied Catalysis B: Environmental 96 (2010) 276–289.
[10] F. Vindigni, M. Manzoli, T. Tabakova, V. Idakiev, F. Boccuzzi, A. Chiorino, Applied Catalysis B: Environmental 125 (2012) 507–515.
[11] P.S. Lambrou, P.G. Savva, J.L.G. Fierro, A.M. Efstathiou, Applied Catalysis B: Environmental 76 (2007) 375–385.
[12] J. Kugai, T. Moriya, S. Seino, T. Nakagawa, Y. Ohkubo, H. Nitani, Y. Mizukoshi, T.A. Yamamoto, Applied Catalysis B: Environmental 126 (2012) 306–314.
[13] C.M. Kalamaras, S. Americanou, A.M. Efstathiou, Journal of Catalysis 279 (2011) 287–300.
[14] A. Martínez-Arias, M. Fernandez-Gawia, A. Hungría, A. Iglesias-Juez, O. Gálvez, J. Anderson, J. Conesa, J. Soria, G. Munuera, Journal of Catalysis 214 (2003) 261–272.
[15] P. Gawade, B. Bayram, A.C. Alexander, U.S. Ozkan, Applied Catalysis B: Environmental 128 (2012) 21–30.
[16] O. Laguna, M. Centeno, M. Boutonnet, J. Odriozola, Applied Catalysis B: Environmental 106 (2011) 621–629.
[17] P.S. Lambrou, A.M. Efstathiou, Journal of Catalysis 240 (2006) 182–193.
[18] A. Gupta, M.S. Hegde, K. Priolkar, U. Waghmare, P. Sarode, S. Emura, Chemistry of Materials 21 (2009) 5836–5847.
[19] G. Dutta, U.V. Waghmare, T. Baidya, M.S. Hegde, K. Priolkar, P. Sarode, Chemistry of Materials 18 (2006) 3249–3256.
[20] M.S. Hegde, G. Madras, K.C. Patil, Accounts of Chemical Research 42 (2009) 704–712.
[21] B. Murugan, A. Ramaswamy, D. Srinivas, C. Gopinath, V. Ramaswamy, Chemistry of Materials 17 (2005) 3983–3993.
[22] P. Singh, M.S. Hegde, Journal of Solid State Chemistry 181 (2008) 3248–3256.
[23] Y. Li, Q. Fu, M. Flytzani-Stephanopoulos, Applied Catalysis B: Environmental 27 (2000) 179–191.
[24] T. Zhu, L. Kundakovic, A. Dreher, M. Flytzani-Stephanopoulos, Catalysis Today 50 (1999) 381–397.
[25] W. Liu, M. Flytzani-Stephanopoulos, Chemical Engineering Journal and Biochemical Engineering Journal 64 (1996) 283–294.
[26] H. Gandhi, G. Graham, R.W. McCabe, Journal of Catalysis 216 (2003) 433–442.
[27] A.B. Kehoe, D.O. Scanlon, G.W. Watson, Chemistry of Materials 23 (2011) 4464–4468.
[28] G. Dutta, U.V. Waghmare, T. Baidya, M.S. Hegde, K. Priolkar, P. Sarode, Catalysis Letters 108 (2006) 165–172.
[29] M. Kurnatowska, L. Kepinski, W. Mista, Applied Catalysis B: Environmental 117–118 (2012) 135–147.
[30] L. Qi, Q. Yu, Y. Dai, C. Tang, L. Liu, H. Zhang, F. Gao, L. Dong, Y. Chen, Applied Catalysis B: Environmental 119–120 (2012) 308–320.
[31] C. Costa, S. Christou, G. Georgiou, A.M. Efstathiou, Journal of Catalysis 219 (2003) 259–272.
[32] H.L. Chen, J.G. Chang, H.T. Chen, Chemical Physics Letters 502 (2011) 169–172.
[33] D.O. Scanlon, G.W. Watson, Physical Chemistry Chemical Physics 13 (2011) 4279–4284.
[34] V.M. Shinde, G. Madras, Applied Catalysis B: Environmental 123 (2012) 367–378.
[35] S. Sharma, Z. Hu, P. Zhang, E.W. McFarland, H. Metiu, Journal of Catalysis 278 (2011) 297–309.
[36] J.P. Holgado, R. Alvarez, G. Munuera, Applied Surface Science 161 (2000) 301–315.
[37] B.M. Reddy, I. Ganesh, E.P. Reddy, Journal of Physical Chemistry B 101 (1997) 1769–1774.
[38] C.N.R. Rao, D.D. Sarma, S. Vasudevan, M.S. Hegde, Proceedings of the Royal Society of London. A. Mathematical and Physical Sciences 367 (1979) 239–252.
[39] T. Mitsui, K. Tsutsui, T. Matsui, R. Kikuchi, K. Eguchi, Applied Catalysis B: Environmental 81 (2008) 56–63.
[40] N.W. Cant, P. Hicks, B. Lennon, Journal of Catalysis 54 (1978) 372–383.
[41] Y.F.Y. Yao, Journal of Catalysis 87 (1984) 152–162.
[42] E. Bekyarova, P. Fornasiero, J. Kašpar, M. Graziani, Catalysis Today 45 (1998) 179–183.
[43] L. Liu, F. Zhou, L. Wang, X. Qi, F. Shi, Y. Deng, Journal of Catalysis 274 (2010) 1–10.
[44] S. Roy, A. Marimuthu, M.S. Hegde, G. Madras, Applied Catalysis B: Environmental 73 (2007) 300–310.
[45] S. Roy, A. Marimuthu, M.S. Hegde, G. Madras, Applied Catalysis B: Environmental 71 (2007) 23–31.
[46] A. Venezia, L. Liotta, G. Pantaleo, V. La Parola, G. Deganello, A. Beck, Z. Koppány, K. Frey, D. Horváth, L. Guczi, Applied Catalysis A: General 251 (2003) 359–368.
[47] P. Singh, M.S. Hegde, Dalton Transactions 39 (2010) 10768–10780.
[48] K.G. Azzam, I.V. Babich, K. Seshan, L. Lefferts, Journal of Catalysis 251 (2007) 163–171.
[49] M.M. Schubert, S. Hackenberg, A.C. van Veen, M. Muhler, V. Plzak, R.J. Behm, Journal of Catalysis 197 (2001) 113–122.
[50] M.B. Boucher, S. Goergen, N. Yi, M. Flytzani-Stephanopoulos, Physical Chemistry Chemical Physics 13 (2011) 2517–2527.
[51] U. Oran, D. Uner, Applied Catalysis B: Environmental 54 (2004) 183–191.
[52] S.H. Oh, G.B. Fisher, J.E. Carpenter, D.W. Goodman, Journal of Catalysis 100 (1986) 360–376.
[53] S.D. Ebbesen, B.L. Mojet, L. Lefferts, Journal of Catalysis 246 (2007) 66–73.
[54] K. Liu, A. Wang, T. Zhang, ACS Catalysis 2 (2012) 1165–1178.
[55] G. Sedmak, S. Hočevar, J. Levec, Journal of Catalysis 213 (2003) 135–150.
[56] D. Widmann, R.J. Behm, Angewandte Chemie International Edition 50 (2011) 10241–10245.
[57] M.A. Vannice, Catalysis Today 123 (2007) 18–22.
[58] C. Rhodes, G.J. Hutching, A.M. Ward, Catalysis Today 23 (1995) 43–58.
[59] S. Eckle, H.G. Anfang, R.J. Behm, Applied Catalysis A: General 391 (2011) 325–333.
[60] P. Panagiotopoulou, D.I. Kondarides, X.E. Verykios, Journal of Physical Chemistry C 115 (2010) 1220–1230.
[61] W. Deng, C. Carpenter, N. Yi, M. Flytzani-Stephanopoulos, Topics in Catalysis 44 (2007) 199–208.
[62] S. Sharma, P.A. Deshpande, M.S. Hegde, G. Madras, Industrial and Engineering Chemistry Research 48 (2009) 6535–6543.
[63] N. Mahadevaiah, P. Singh, B.D. Mukri, S.K. Parida, M.S. Hegde, Applied Catalysis B: Environmental 108–109 (2011) 117–126.
[64] R. Leppelt, B. Schumacher B, V. Plzak, M. Kinne, R. Behm, Journal of Catalysis 244 (2006) 137–152.
[65] V.M. Shinde, G. Madras, International Journal of Hydrogen Energy 37 (2012) 18798–18814.
[66] R. Gorte, S. Zhao, Catalysis Today 104 (2005) 18–24.
[67] S. Hilaire, X. Wang, T. Luo, R. Gorte, J. Wagner, Applied Catalysis A: General 215 (2001) 271–278.
[68] A. Satsuma, M. Yanagihara, J. Ohyama, K. Shimizu, Catalysis Today 201 (2013) 62–67.